Dalton Transactions

PAPER

View Article Online
View Journal | View Issue

Open Access Article. Published on 09 October 2015. Downloaded on 6/3/2026 2:54:56 PM.
This article is licensed under a Creative Commons Attribution 3.0 Unported Licence.

Cite this: *Dalton Trans.*, 2015, **44**, 20045

A new class of deep-blue emitting Cu(I) compounds – effects of counter ions on the emission behavior†

Timo Gneuß,‡[a] Markus J. Leitl,‡[b] Lars H. Finger,[a] Hartmut Yersin*[b] and Jörg Sundermeyer*[a]

Received 8th August 2015,
Accepted 9th October 2015

DOI: 10.1039/c5dt03065j

www.rsc.org/dalton

Three deep blue emitting Cu(I) compounds, [Cu(PPh$_3$)tpym]PF$_6$, [Cu(PPh$_3$)tpym]BF$_4$, and [Cu(PPh$_3$)tpym]BPh$_4$ (tpym = tris(2-pyridyl)methane, PPh$_3$ = triphenylphosphine) featuring the tripodally coordinating tpym and the monodentate PPh$_3$ ligands were studied with regard to their structural and photophysical properties. The compounds only differ in their respective counter ions which have a strong impact on the emission properties of the powder samples. For example, the emission quantum yield can be significantly increased for the neat material from less than 10% to more than 40% by exchanging BPh_4^- with PF_6^-. These effects can be linked to different molecular packings which depend on the counter ion. In agreement with these results, it was found that the emission properties also strongly depend on the surrounding matrix environment which was elucidated by investigating photophysical properties of the compounds as powders, doped into a polymer matrix, and dissolved in a fluid solution, respectively. The observed differences in the emission behavior can be explained by different and pronounced distortions that occur in the excited state. These distortions are also displayed by density functional theory (DFT) calculations.

Introduction

In the last few decades, significant research attention has been devoted to the development of new emitter materials for organic light-emitting diodes (OLEDs) and light-emitting electrochemical cells (LEECs).[1–14] A breakthrough in this field was achieved when the potential of 3rd row transition metal complexes was recognized for these applications. Such compounds can display strong spin–orbit coupling (SOC) which can result in high phosphorescence emission quantum yields and short emission decay times of only a few microseconds.[9,15–18] Most importantly, the involvement of the triplet state in the emission process and the fast intersystem crossing (ISC) from the lowest excited singlet to the lowest triplet state allow the use of all injected excitons, singlets and triplets, for the generation of light in electroluminescent devices through the triplet harvesting effect.[19–21] As a consequence, the efficiency increases by a factor of four compared to conventional purely organic, fluorescent emitters which can only utilize singlet excitons. However, efficient triplet emitters are based on expensive and rare noble metals such as iridium and platinum.[1,4,5,7–9,11,13,16,21–29] Furthermore, developing efficient and long-term stable blue light emitters with this class of compounds remains challenging due to energetically relatively low-lying metal centered dd* states that provide a path for non-radiative decay to the ground state or even molecular decomposition.[30]

In recent years, compounds based on low-cost and more abundant 1st row transition metal copper have come into the focus of research.[9,10,14,31–38] At first sight, emitters based on Cu(I) seem rather unsuitable for application in electroluminescent devices due to the significantly smaller SOC constant of copper compared to platinum or iridium,[39] for example. Thus, Cu(I) complexes frequently exhibit triplet decay times of several 100 microseconds or more.[9,14,22,31–33,35,40–49] This would lead to pronounced saturation effects, if these materials are applied as emitters in electroluminescent devices.[50] However, the long triplet decay time is not effective if the compounds exhibit only a small energy separation $\Delta E(S_1–T_1)$ between the first excited singlet S_1 and the triplet state T_1. Then, an efficient thermal population (up-ISC) of the S_1 state from the energetically lower lying T_1 state can occur at

[a]*Philipps-Universität Marburg, Materials Science Centre and Fachbereich Chemie, Hans-Meerwein-Straße 4, 35032 Marburg, Germany. E-mail: jsu@staff.uni-marburg.de; Fax: +49 (0)6421 28-25711; Tel: +49 (0)6421 28-25693*

[b]*Universität Regensburg, Institut für Physikalische und Theoretische Chemie, Universitätsstr. 31, 93053 Regensburg, Germany. E-mail: hartmut.yersin@ur.de; Fax: +49 (0)941 943-4488; Tel: +49 (0)941 943-4464*

†Electronic supplementary information (ESI) available: Parts of the crystal structures and NMR spectra of **1–3** are given in Fig. S1–S11. CCDC 1415676–1415678. For ESI and crystallographic data in CIF or other electronic format see DOI: 10.1039/c5dt03065j

‡These authors contributed equally to this work.

Open Access Article. Published on 09 October 2015. Downloaded on 6/3/2026 2:54:56 PM.
This article is licensed under a Creative Commons Attribution 3.0 Unported Licence.

ambient temperature. As the spin-allowed $S_1 \rightarrow S_0$ transition shows a significantly higher oscillator strength than the spin-forbidden $T_1 \rightarrow S_0$ transition, the overall decay time decreases distinctly by this process and decay times of only a few μs can be reached.[9,14,22,31–35,40–45,51,52] This emission mechanism corresponds to a thermally activated delayed fluorescence (TADF).[53] In an electroluminescent device, this mechanism allows utilizing all injected excitons for the generation of light. Accordingly, the excitation is harvested and emitted essentially *via* the singlet S_1 state. Thus, this mechanism is called the singlet harvesting effect.[9,14,22,31–33,35,40,54–56] Additionally, in Cu(I) complexes the d-shell of the copper ion is fully occupied (d^{10} electron configuration) and therefore, low-lying dd* states that could quench the emission and would be a source of molecular decomposition do not occur. This renders Cu(I) complexes promising candidates for the realization of efficient and long-term stable blue light emitters for OLEDs and LEECs.

Compared to emitters based on Pt(II) and Ir(III), which preferably exhibit square-planar or octahedral coordination geometries, respectively, Cu(I) compounds show a richer structural diversity.[14,31–36,38,40,43,45,54,56–80] However, so far photophysical investigations have been mainly focused on mononuclear complexes with two bidentate ligands,[32,33,37,40,70–72,77–83] mononuclear complexes with one mono and one bidentate ligand,[34,38,43,63–65] and on dinuclear complexes in which the two copper centers are bridged by halides.[14,35,36,56,59–62] To our knowledge, only very few Cu(I) complexes with tripodal ligands have been studied with regard to their photophysical properties.[54,57,58]

Herein, we report the new cationic tripodally coordinated deep-blue emitting Cu(I) complex $[Cu(PPh_3)tpym]^+$ (PPh_3 = triphenylphosphine, tpym = tris(2-pyridyl)methane). Interestingly, the emission properties distinctly depend on the counter ion. Therefore, we discuss properties of the three powder materials $[Cu(PPh_3)tpym]PF_6$ (**1**), $[Cu(PPh_3)tpym]BF_4$ (**2**), and $[Cu(PPh_3)tpym]BPh_4$ (**3**) and compare the results with those for the compounds doped into polymethylmethacrylate (PMMA). All compounds were characterized chemically by NMR spectroscopy, IR spectroscopy, mass spectrometry, elemental analysis, and X-ray analysis. In addition, density functional theory (DFT) and time-dependent density functional theory (TDDFT) calculations were performed for the cationic part $[Cu(PPh_3)tpym]^+$ to gain further insight into the electronic structure of this complex.

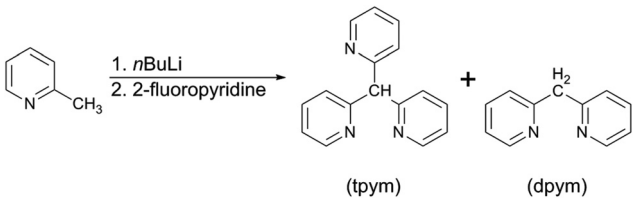

Scheme 1 Synthesis of the methane derivative tris(2-pyridyl)methane (tpym) according to ref. 84.

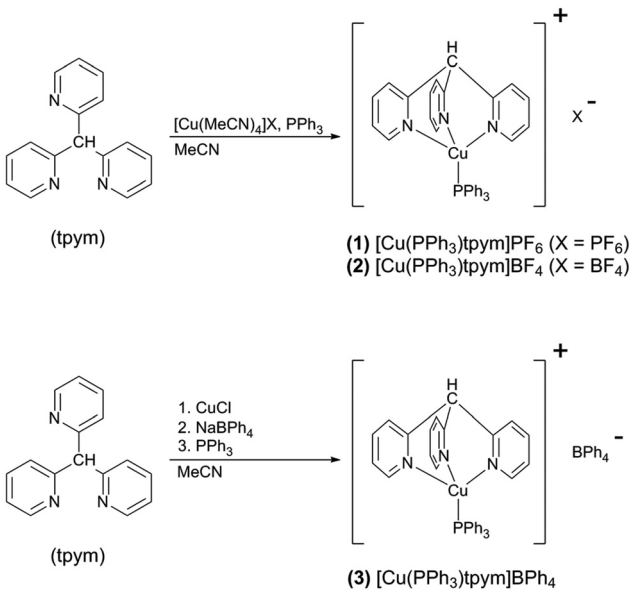

Scheme 2 Synthesis of the copper(I) compounds.

Results and discussion

Synthesis

The copper(I) compounds $[Cu(PPh_3)tpym]PF_6$ (**1**), $[Cu(PPh_3)tpym]BF_4$ (**2**), and $[Cu(PPh_3)tpym]BPh_4$ (**3**) were prepared in a two-step synthesis. In the first step, the tripodal ligand tris(2-pyridyl)methane (tpym) was prepared according to a literature method (Scheme 1).[84] In the second step, compounds **1** and **2** were synthesized by reaction of the corresponding copper(I) salts $[Cu(MeCN)_4]PF_6$ and $[Cu(MeCN)_4]BF_4$, respectively, with PPh_3 and tpym. The yields for both compounds are quantitative. Compound **3** was prepared with an overall yield of 35% in three *in situ* steps (Scheme 2). In the first step, the complex [Cu(Cl)tpym] was formed by reaction of CuCl with tpym. Then, by adding $NaBPh_4$ an anion exchange between the chloride and the tetraphenylborate anion is accomplished. Finally, by adding PPh_3 compound **3** was obtained.

X-ray crystal structures

Single crystals suitable for X-ray structure determination could be obtained for all three investigated compounds (**1**, **2**, and **3**) from a saturated chloroform solution by layering with *n*-pentane at ambient temperature. The crystallographic data and structure refinement details are summarized in Table 1; selected bond distances and angles are listed in Table 2. The molecular structures of **1–3** are shown in Fig. 1. The three compounds crystallize in different crystal systems, compound **1** in the monoclinic, compound **2** in the trigonal, and compound **3** in the orthorhombic crystal system.

 This journal is © The Royal Society of Chemistry 2015

Open Access Article. Published on 09 October 2015. Downloaded on 6/3/2026 2:54:56 PM.
This article is licensed under a Creative Commons Attribution 3.0 Unported Licence.

Table 1 Crystallographic data for compounds **1–3**

	1 $[Cu(PPh_3)tpym]PF_6{\cdot}CHCl_3$	**2** $[Cu(PPh_3)tpym]BF_4{\cdot}0.5\ CHCl_3$	**3** $[Cu(PPh_3)tpym]BPh_4{\cdot}2\ CHCl_3$
Habitus	Plate	Needle	Plate
Color	Colorless	Colorless	Colorless
Formula	$C_{35}H_{29}Cl_3CuF_6N_3P_2$	$C_{34.50}H_{28.50}BCl_{1.50}CuF_4N_3P$	$C_{60}H_{50}BCl_6CuN_3P$
fw [g mol^{-1}]	837.44	719.60	1131.05
Crystal size [mm^3]	0.220 × 0.180 × 0.090	0.291 × 0.043 × 0.041	0.319 × 0.267 × 0.064
Crystal system	Monoclinic	Trigonal	Orthorhombic
Space group	$P2_1$	$R\bar{3}c$	$Pna2_1$
a [Å]	8.5970(3)	12.8635(6)	19.4837(7)
b [Å]	18.9423(8)	12.8635	11.1499(4)
c [Å]	11.5950(5)	67.361(3)	24.6713(9)
α [°]	90	90	90
β [°]	107.2000(10)	90	90
γ [°]	90	120	90
Cell volume [Å^3]	1803.77(13)	9652.9(10)	5359.6(3)
Z	2	12	4
D_{calc} [Mg m^{-3}]	1.542	1.485	1.402
Abs. coeff. [mm^{-1}]	0.978	0.907	0.780
F(000)	848	4404	2328
T [K]	100(2)	100(2)	100(2)
λ [Å]	0.71069	0.71069	0.71069
Reflns collected	26 555	28 280	54 250
Indep. reflns	7884	2458	11 572
Obs. reflns [$I > 2(I)$]	7265	1742	9836
Reflns used for refin.	7884	2458	11 572
Abs. correction	Multi-scan	Multi-scan	Multi-scan
GOF	1.030	1.037	1.069
wR_2	0.0643	0.0958	0.0662
R_1 [$I > 2\sigma(I)$]	0.0290	0.0383	0.0294

Table 2 Selected bond distances [Å] and angles [°] for compounds **1–3**

	1	**2**[a]	**3**
Cu1–N1	2.047(3)	2.073(2)	2.056(3)
Cu1–N2	2.080(3)	2.073(2)	2.048(3)
Cu1–N3	2.075(3)	2.073(2)	2.098(3)
Cu1–P1	2.160(1)	2.158(1)	2.152(1)
C16–C1	1.527(4)	1.522(3)	1.520(4)
C16–C6	1.524(4)	1.522(3)	1.526(4)
C16–C11	1.520(4)	1.522(3)	1.518(4)
P1–Cu1–N1	124.9(1)	125.3(1)	132.1(1)
P1–Cu1–N2	123.4(1)	125.3(1)	120.3(1)
P1–Cu1–N3	127.5(1)	125.3(1)	121.3(1)
N1–Cu1–N2	89.6(1)	90.0(1)	90.4(1)
N1–Cu1–N3	91.1(1)	90.0(1)	89.2(1)
N2–Cu1–N3	89.1(1)	90.0(1)	92.3(1)
P1–Cu1–C16	177.6(0)	180.0(0)	172.6(1)

[a] Since compound **2** crystallizes in the space group $R\bar{3}c$, the pyridine and phenyl groups are crystallographically imposed symmetry equivalent with respect to each other. Nevertheless, for better comparability we use the same atom labeling scheme for compound **2** as for **1** and **3**.

The copper(I) centers are coordinated by the phosphine ligand PPh_3 and the three N atoms of tpym in a distorted tetrahedral configuration. The bending of the PPh_3 ligand from the C16–Cu1 axis (compare Fig. 1) is different for the three compounds. For compound **2**, there is no bending of the PPh_3 ligand (P1–Cu1–C16 = 180.0(0)°). For compound **1**, with an angle of P1–Cu1–C16 = 177.6 (0)°, the PPh_3 bending is small, but for compound **3**, with an angle of P1–Cu1–C16 = 172.6 (1)°, the bending is clearly displayed. Thus it seems that the bending of the PPh_3 ligand from the C16–Cu1 axis increases with the increasing size of the counter anion (BF_4 < PF_6 < BPh_4). The crystal packing diagram of compound **3** with the most pronounced PPh_3 bending reveals that this bending is a result of the interaction of the PPh_3 ligand with the counter anion BPh_4 (see Fig. S3, ESI†). One phenyl group of BPh_4 is directly oriented towards the PPh_3 ligand of the adjacent copper complex. The resulting steric repulsion is decreased by the bending of the PPh_3 ligand. For compounds **1** and **2** with the smaller counter anions PF_6 and BF_4, the interaction of the PPh_3 group of the Cu(I) complex with its neighboring molecules is rather balanced. This can be supported by the performed DFT calculations (see below) which indicate that in the absence of counter ions and neighboring molecules the angle P1–Cu1–C16 amounts to 180°.

It is remarked that we have performed similar investigations for neutral Cu(I) complexes with tripodal ligands (similar to tpym) previously but with a halide (Cl, Br, or I) instead of the PPh_3 ligand at the fourth coordination site. Also for these compounds a bending of the monodentate (halide) ligand has been observed in the crystal structures.[54]

Computational studies

Quantum chemical calculations have been carried out for the cationic complex $[Cu(PPh_3)tpym]^+$ using density functional theory (DFT) and time-dependent density functional theory (TDDFT) with the hybrid functional B3LYP[85–87] and the basis

Open Access Article. Published on 09 October 2015. Downloaded on 6/3/2026 2:54:56 PM.
This article is licensed under a Creative Commons Attribution 3.0 Unported Licence.

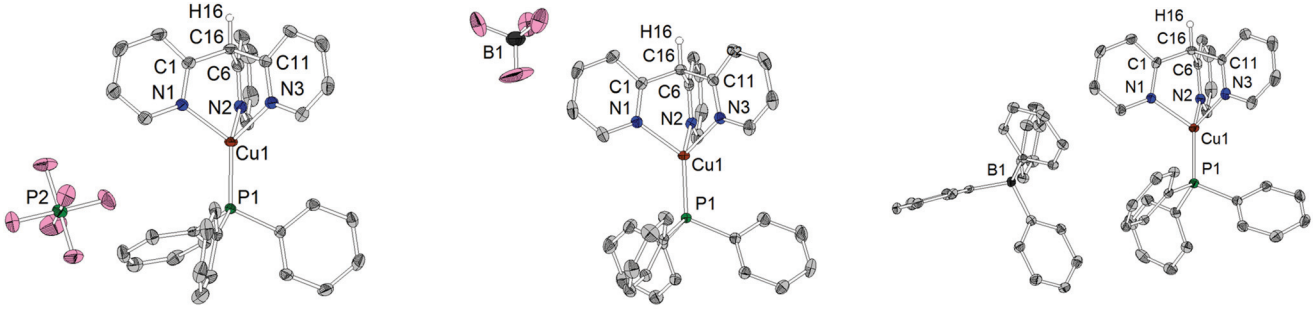

[Cu(PPh$_3$)tpym]PF$_6$ (**1**) [Cu(PPh$_3$)tpym]BF$_4$ (**2**) [Cu(PPh$_3$)tpym]BPh$_4$ (**3**)

Fig. 1 Molecular structures of **1–3** (thermal ellipsoids with 50% probability) resulting from X-ray analyses. Hydrogen atoms (except for H16) and solvent molecules are omitted for clarity.

set def2-SVP.[88,89] For [Cu(PPh$_3$)tpym]$^+$, the ground state (S_0), the first excited triplet state (T_1), and the first excited singlet state (S_1) geometries were calculated. The results are displayed in Fig. 2. Frequency calculations confirm that these three optimized structures are minima on the potential energy surface.

For the S_0 geometry, it was found that the atom P1 of the PPh$_3$ group lies on the axis that is defined by the atoms C16 and Cu1 (Fig. 2a) (angle P1–Cu1–C16 = 180°). The bond lengths of the three Cu–N bonds are almost equal, amounting to 2.137 Å (Cu1–N1), 2.137 Å (Cu1–N2), and 2.139 Å (Cu1–N3). However, in the T_1 (Fig. 2b) and S_1 state geometries (Fig. 2c), the P1 atom, and thus, the whole PPh$_3$ group, is bent away from the C16–Cu1 axis. For the T_1 geometry, the PPh$_3$ group is angled by about 26° (P1–Cu1–C16 = 153.8°) and for the S_1 geometry by about 30° (P1–Cu1–C16 = 149.7°). Also, the three Cu–N bonds are no longer equal in the excited state geometries. In the T_1 geometry, two Cu–N bonds are significantly shorter than in the S_0 geometry, with bond lengths amounting to Cu1–N1 = 2.000 Å and Cu1–N2 = 1.965 Å, whereas the length of the third copper–nitrogen bond increases to Cu1–N3 = 2.167 Å. On the other hand, for the S_1 geometry two Cu–N bonds become longer, with two equal bond lengths of Cu1–N1 = 2.149 Å and Cu1–N3 = 2.149 Å, and one Cu–N bond becomes significantly shorter, with a bond length of Cu1–N2 = 1.986 Å. These data and other important bond lengths and angles are summarized in Table 3.

Furthermore, it was found that the highest occupied molecular orbital (HOMO) is mainly located at the Cu(I) center whereas the lowest unoccupied molecular orbital (LUMO) is distributed over two of the three pyridine moieties of the tpym ligand (compare Fig. 3).

Table 3 Selected calculated bond distances [Å] and angles [°] for the ground state (S_0), the first excited triplet state (T_1), and the first excited singlet state (S_1) geometry of [Cu(PPh$_3$)tpym]$^+$

	S_0	T_1	S_1
Cu1–N1	2.137	2.000	2.149
Cu1–N2	2.137	1.965	1.986
Cu1–N3	2.139	2.167	2.149
Cu1–P1	2.242	2.356	2.339
P1–Cu1–N1	125.9	108.4	106.4
P1–Cu1–N2	125.9	150.0	154.8
P1–Cu1–N3	126.4	110.3	107.8
N1–Cu1–N2	88.9	89.2	90.0
N1–Cu1–N3	88.9	97.4	93.2
N2–Cu1–N3	88.9	90.5	89.8
P1–Cu1–C16	179.7	153.8	149.7

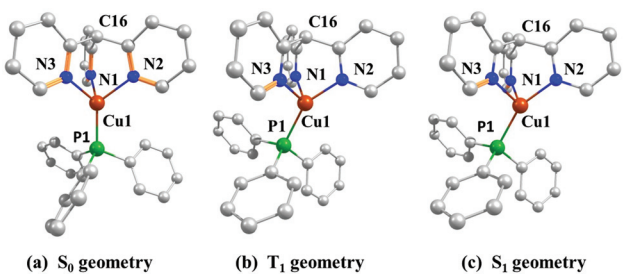

(a) S_0 geometry (b) T_1 geometry (c) S_1 geometry

Fig. 2 Optimized geometries of the ground state S_0 (a), the first excited triplet state T_1 (b), and the first excited singlet state S_1 (c) of [Cu(PPh$_3$)tpym]$^+$. Calculations were performed on the B3LYP/def2-SVP level of theory. All hydrogen atoms are omitted for clarity.

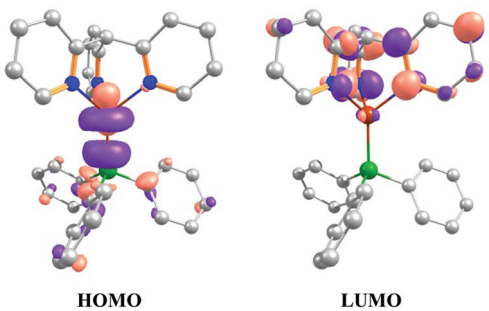

HOMO LUMO

Fig. 3 Highest occupied (HOMO) and lowest unoccupied molecular orbitals (LUMO) for [Cu(PPh$_3$)tpym]$^+$ calculated for the ground state geometry. Calculations were performed on the B3LYP/def2-SVP level of theory. All hydrogen atoms are omitted for clarity.

This journal is © The Royal Society of Chemistry 2015

Open Access Article. Published on 09 October 2015. Downloaded on 6/3/2026 2:54:56 PM.
This article is licensed under a Creative Commons Attribution 3.0 Unported Licence.

TDDFT calculations reveal that transitions between these two frontier orbitals largely determine the first excited singlet S_1 and triplet T_1 states which leads to the assignment of these states as metal-to-ligand charge-transfer (MLCT) states. This allows us to give an explanation for the occurrence of geometry distortions in the S_1 and T_1 states: On excitation, a significant amount of charge is transferred from the Cu(I) metal center to the ligand. As a consequence, the copper center is formally partially oxidized from Cu(I) to Cu(II). As Cu(II) prefers a planar coordination environment in contrast to Cu(I) (which favors tetrahedral coordination), such an oxidation is connected with pronounced structural reorganizations. For example, for Cu(I) complexes with two bidentate ligands, this is displayed by a flattening distortion from a tetrahedral to a more planar coordination geometry.[71,77,90–92] In the case of the cationic Cu(I) complex presented in this study, the distortion is represented by the bending of the PPh_3 group as described above.

The pronounced charge transfer character of the S_1 and T_1 states has another important consequence. Due to the distinct spatial separation of HOMO and LUMO, the spatial overlap between these two frontier orbitals is small. As a consequence, the exchange integral is also small. Accordingly, the energy separation $\Delta E(S_1–T_1)$ between the first excited singlet and triplet state is small. From TDDFT calculations it was found that this energy separation amounts only to $\Delta E(S_1–T_1) = 810\ cm^{-1}$. For such a small energy splitting a thermally activated delayed fluorescence (TADF) is expected to occur at ambient temperature, which is also indicated by the studies presented below.

Photophysical studies

In Fig. 4, electronic absorption spectra of the compounds [Cu(PPh$_3$)tpym]PF$_6$ (**1**), [Cu(PPh$_3$)tpym]BF$_4$ (**2**), and [Cu(PPh$_3$)tpym]BPh$_4$ (**3**) are displayed. In addition, the absorption spectra of the tpym and the PPh_3 ligands are also shown. All spectra were recorded under ambient conditions for the compounds dissolved in dichloromethane, except for PPh_3 for which the absorption was measured in acetonitrile.[93]

The absorption spectra of compounds **1–3** show similar spectral shapes. All spectra exhibit intense high energy absorption bands in the wavelength region below 280 nm with peaks at 229 nm, 248 nm, and 260 nm, respectively. The corresponding electronic transitions are identified to originate from ligand centered (LC) π–π* transitions of the tpym and the PPh_3 ligands, which show intense absorptions in this spectral range. At longer wavelengths, distinctly weaker absorption bands are observed which are not present in the spectrum of the tpym or PPh_3 ligands. Therefore, these bands can be attributed to transitions that are of metal-to-ligand charge transfer (MLCT) character. This assignment is also in agreement with DFT and TDDFT calculations discussed in the previous section which predict low lying MLCT states and agrees with literature reports of other Cu(I) complexes.[9,14,22,33,40–45,51,52]

It is not surprising that the absorption spectra of all three compounds exhibit similar spectral shapes as the investigated substances differ only in their respective counter anions. In a dilute solution, the counter anions do not interact with the Cu(I) complexes and therefore, do not influence the absorption behavior. Furthermore, the BF_4^- and PF_6^- ions are not expected to show absorption in the investigated wavelength range. In contrast, the phenyl groups of BPh_4^- show distinct absorption in the wavelength range between 230 nm and 260 nm which explains the differences in the spectra of substance **3** when compared to those of **1** and **2**.

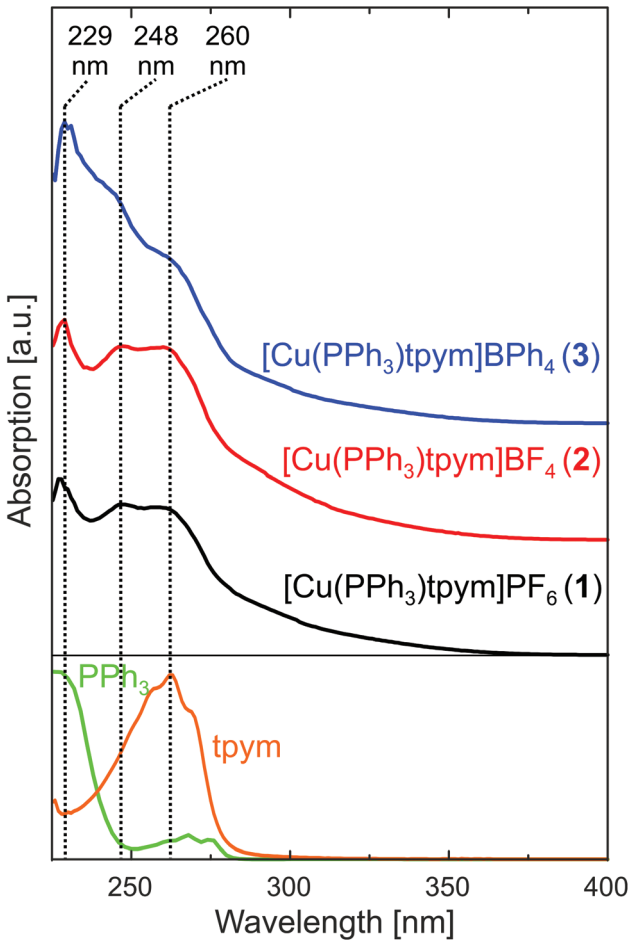

Fig. 4 Absorption spectra of the three compounds **1–3** and the tpym ligand recorded in dichloromethane solution under ambient conditions. PPh_3 absorption has been measured under the same conditions but in acetonitrile solution.[93]

In fluid dichloromethane (DCM) solution, the Cu(I) complexes are not emissive at ambient temperature, even if oxygen is carefully removed from the solution by repeatedly applying a freeze–pump–thaw process. In contrast, emission is observed for complexes doped into a polymethylmethacrylate (PMMA) matrix. The corresponding emission spectra are displayed in Fig. 5 and are found to be essentially identical for all the compounds. They are broad and featureless, being in agreement with the MLCT character of the emissive state,[31–35,40,63–65] with a peak at $\lambda_{max} = 470$ nm. Also, the emission quantum yield of $\Phi_{PL} = 7\%$ is equal for all the compounds (compare Table 4). These results show that the counter anions do not have an influence on the emission behavior of the Cu(I) complexes

Open Access Article. Published on 09 October 2015. Downloaded on 6/3/2026 2:54:56 PM.
This article is licensed under a Creative Commons Attribution 3.0 Unported Licence.

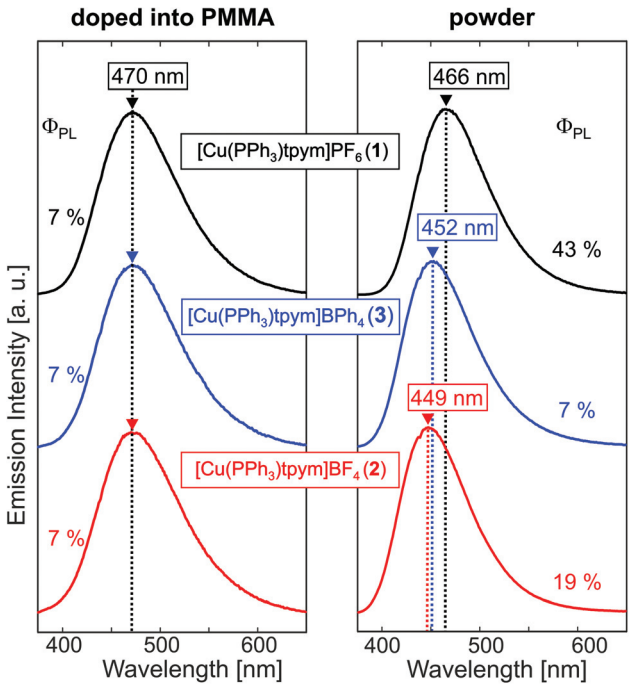

Fig. 5 Normalized emission spectra of the investigated compounds **1–3** doped into a PMMA matrix and as powders. All spectra were recorded under ambient conditions. The samples were excited at λ_{exc} = 350 nm.

Table 4 Emission properties of $[Cu(PPh_3)tpym]PF_6$ (**1**), $[Cu(PPh_3)tpym]BF_4$ (**2**) and $[Cu(PPh_3)tpym]BPh_4$ (**3**) powders at 300 K and 77 K. λ_{max} represents the wavelength at the maximum of the emission spectrum, τ the emission decay time, and Φ_{PL} the photoluminescence quantum yield. The radiative rate k_r and the nonradiative rate k_{nr} were calculated according to $k_r = \Phi_{PL}\,\tau^{-1}$ and $k_{nr} = (1-\Phi_{PL})\,\tau^{-1}$, respectively. The asterisk (*) indicates that the decay behavior deviates slightly from a mono-exponential decay. Decay times for the compounds doped into a PMMA matrix deviate significantly from a mono-exponential behavior. For this reason, no τ value is given for the PMMA samples

		1	**2**	**3**
Powder	λ_{max} (300 K) [nm]	466	449	452
	τ (300 K) [μs]	14	7.5*	5.4*
	Φ_{PL} (300 K) [%]	43	19	7
	k_r (300 K) [s^{-1}]	3.1×10^4	2.5×10^4	1.3×10^4
	k_{nr} (300 K) [s^{-1}]	4.1×10^4	1.1×10^5	1.7×10^5
	λ_{max} (77 K) [nm]	478	462	462
	τ (77 K) [μs]	26	19*	25*
PMMA	λ_{max} (300 K) [nm]	470	470	470
	Φ_{PL} (300 K) [%]	7	7	7

doped into the PMMA matrix which presumably is due to the spatial separation of the counter anions and the Cu(I) complex in the PMMA matrix at low doping concentrations. The relatively small value of Φ_{PL} is related to the non-rigid environment in the PMMA polymer. This allows significant quenching of the excited states as explained below. Interestingly, for the powder samples with different counter anions one finds distinct differences in the emission properties. The spectra of the three compounds are clearly shifted relative to each other with emission maxima lying at $\lambda_{max}(\mathbf{1})$ = 466 nm, $\lambda_{max}(\mathbf{2})$ = 449 nm, and $\lambda_{max}(\mathbf{3})$ = 452 nm (Fig. 5). Also, the emission quantum yields vary distinctly amounting to $\Phi_{PL}(\mathbf{1})$ = 43%, $\Phi_{PL}(\mathbf{2})$ = 19%, and $\Phi_{PL}(\mathbf{3})$ = 7%, at ambient temperature.

Presumably, these differences are a consequence of the interaction of the counter anions with the Cu(I) complex due to their proximity in the solid phase. In the crystals of the compounds, these interactions are displayed in different packings and different geometries of the $[Cu(PPh_3)tpym]^+$ complex, depending on the counter anion (compare crystal structures discussed above and ESI Fig. S1–S3†). For example, the orientation of the PPh_3 group compared to the rest of the molecules is strongly dependent on the counter anion and thus, influences the emission properties. Similar effects have been investigated previously.[94–97] It is reasonable to assume that in the powder phase, the counter anions have similar effects on the compounds' geometries.

A comparison of the emission properties in different matrices reveals an interesting trend. In the powder phase, compound **1** exhibits an emission quantum yield of 43%, but when doped into a PMMA matrix the quantum yield amounts only to 7% and in solution, the quantum yield is ≪1%. This is related to increasing distortions that Cu(I) complexes undergo on excitation with decreasing matrix rigidity.[9,31,40,55,60] As already discussed in the previous section, the compounds show structural distortion on excitation, especially, a bending of the PPh_3 group away from the C16–Cu1 axis. As a consequence, the potential energy curves for the excited and the ground states are shifted with respect to each other. Accordingly, the non-radiative rate increases due to an increase of the Franck–Condon factors that govern these deactivation processes to the ground state.[9,31,98,99] In matrices with low rigidity, such as fluid solutions, this effect is particularly pronounced. In more rigid environments, geometry distortions are much less distinct resulting in higher quantum yields. In powder, geometry distortions upon excitation are partly suppressed resulting in higher quantum yields of the Cu(I) compounds. Interestingly, here it is shown that also the counter anion (and the resulting molecular packing) has an influence on the emission quantum yield of the powder samples. Thus, the counter anions prevent large geometry distortions if they limit the available space for distortions in the molecular packing.

It is remarked that the emission spectra of the compounds as powders show a clear blue shift of the order of 10 nm on heating from T = 77 K to ambient temperature (**1**: 540 cm^{-1}, **2**: 620 cm^{-1}, **3**: 480 cm^{-1}). This is an indication that a thermally activated delayed fluorescence (TADF) occurs. According to this emission mechanism, the singlet state S_1 is populated at ambient temperature and contributes to the emission (Fig. 6). As this state lies energetically higher, a blue shift of the emission with increasing temperature is expected. The energy separation of $\Delta E(S_1–T_1)$ = 810 cm^{-1}, as found from TDDFT calculations, is in fairly good agreement with the experimental values resulting from the spectral shifts and therefore supports this assignment. Furthermore, the thermal population of the

This journal is © The Royal Society of Chemistry 2015

Open Access Article. Published on 09 October 2015. Downloaded on 6/3/2026 2:54:56 PM.
This article is licensed under a Creative Commons Attribution 3.0 Unported Licence.

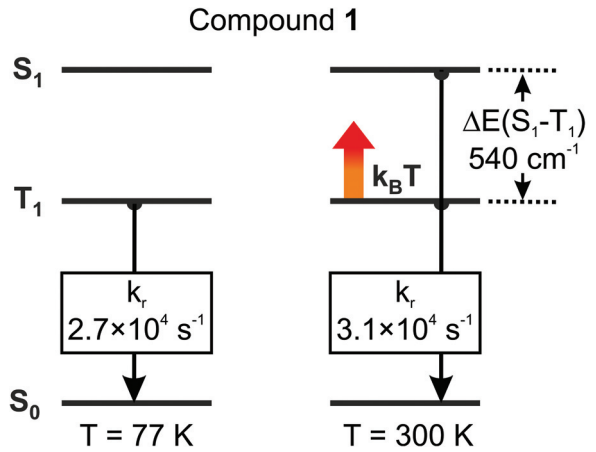

Fig. 6 Emission decay paths for compound **1** at different temperatures. At low temperatures (T = 77 K), only the lowest excited triplet state T_1 emits, while at ambient temperature (T = 300 K), an *additional* radiative decay path *via* thermal population of the S_1 state is opened.

singlet state should result in an increase of the radiative rate on heating as the spin-allowed $S_1 \rightarrow S_0$ transition carries significantly more allowedness than the spin-forbidden $T_1 \rightarrow S_0$ transition. Indeed, on heating, a slight increase of the radiative rate from k_r (77 K) = 2.7 × 10^4 s^{-1} to k_r (300 K) = 3.1 × 10^4 s^{-1} is observed for compound **1**. However, this increase is smaller than that observed for other TADF materials. Presumably, this is mainly due to the fact that the triplet state itself exhibits comparably fast deactivation to the ground state with a decay time of only 26 μs for compound **1**. This value is significantly shorter than that found for other TADF systems for which triplet decay times can be several hundred μs or even longer.[31–33,41]

Conclusion and outlook

In this contribution, we have presented a new class of emitter materials based on a Cu(I) complex with a tripodal ligand. As powders, the three compounds [Cu(PPh$_3$)tpym]X (X = PF_6 (**1**), BF_4 (**2**), and BPh_4 (**3**)) display bright emission in the deep-blue range of the spectrum. For example, at ambient temperature, the emission of [Cu(PPh$_3$)tpym]PF_6 (**1**) peaks at 466 nm and the emission quantum yield amounts to 43%. However, if this compound is doped into a polymer PMMA matrix, the emission is slightly red-shifted to 470 nm, but the quantum yield is drastically reduced to 7%. In fluid dichloromethane solution, the compound is not emissive. This indicates that molecular reorganizations on excitation which can easily occur in non-rigid environments are a major source of non-radiative relaxation to the ground state. For other Cu(I) compounds, it has been shown that limiting such distortions can lead to drastic increases of the emission quantum yields even in solution. For example, for the cationic complexes [Cu(POP)(dmbpy)]$^+$ and [Cu(POP)(tmbpy)]$^+$ (POP = bis[2-(diphenylphosphino)-phenyl]-ether, dmbpy = 4,4′-dimethyl-2,2′-bipyridyl, tmbyp = 4,4′,6,6′-tetramethyl-2,2′-bipyridyl)[40] it has been demonstrated that the introduction of two sterically demanding methyl groups can significantly reduce geometry distortions on excitation and therefore, cause a drastic increase of the emission quantum yield by almost a factor of ten. This strategy could also be applied in future investigations to increase the quantum yield of the compounds presented in this study, for example, by introducing sterically demanding groups that prohibit the bending distortion of the triphenylphosphine group.

Furthermore, we have demonstrated that different counter ions and molecular packings can have a strong impact on the emission behavior of solid samples. For example, the powder of the compound [Cu(PPh$_3$)tpym]PF_6 exhibits an emission quantum yield of 43% and an emission maximum of 466 nm at ambient temperature, whereas for [Cu(PPh$_3$)tpym]BPh_4 the emission is blue shifted to 452 nm and the emission quantum yield is decreased to 7%. These results should be taken into consideration, if solid state samples of other Cu(I) complexes are being investigated.

Experimental

General remarks

Syntheses and handling of air- and moisture-sensitive substances were carried out using standard Schlenk- and glove-box-techniques. Solvents were dried using standard procedures[100] and stored over Al_2O_3/molecular sieves 3 Å/R3-11G catalyst (BASF). The starting materials were obtained from commercial sources and used as received. The following materials were prepared according to literature procedures: Copper(I) chloride,[101] tetrakis(acetonitrile)copper(I) hexafluorophosphate,[102] tetrakis(acetonitrile)copper(I) tetrafluoroborate,[103] and tris(2-pyridyl)methane (tpym).[84]

NMR spectra were recorded at 300 K on a Bruker DPX 250, Bruker ARX 300, Bruker DRX 400, Bruker ARX 500, or Bruker DRX 500 using $CDCl_3$ or CD_3CN as the solvent. Chemical shifts are given with respect to tetramethylsilane (^{1}H, ^{13}C) and 85% phosphoric acid (^{31}P). Calibration of ^{1}H and ^{13}C NMR spectra was accomplished with the deuterated solvent residual signals. ^{31}P NMR spectra were calibrated externally (phosphoric acid). The numbering of the hydrogen and carbon atoms of the three compounds is shown in Fig. 7.

Electrospray ionization (ESI) mass spectra were recorded on a Thermo Fisher Scientific LTQ FT Ultra using acetonitrile as the solvent. IR spectra were recorded on a Bruker Alpha FT-IR spectrometer using powder samples at ambient temperature. Intensities of the bands were characterized as follows: vs = very strong (0–50% transmission), s = strong (50–70% transmission), m = medium (70–90% transmission), w = weak (90–100% transmission). Elemental analysis was performed on an Elementar vario MICRO cube.

UV-Vis absorption measurements were carried out using a Varian Cary 300 double beam spectrometer. Emission spectra were recorded with a Fluorolog 3-22 (Horiba Jobin Yvon) spectrophotometer which was equipped with a cooled photo-multi-

Open Access Article. Published on 09 October 2015. Downloaded on 6/3/2026 2:54:56 PM.
This article is licensed under a Creative Commons Attribution 3.0 Unported Licence.

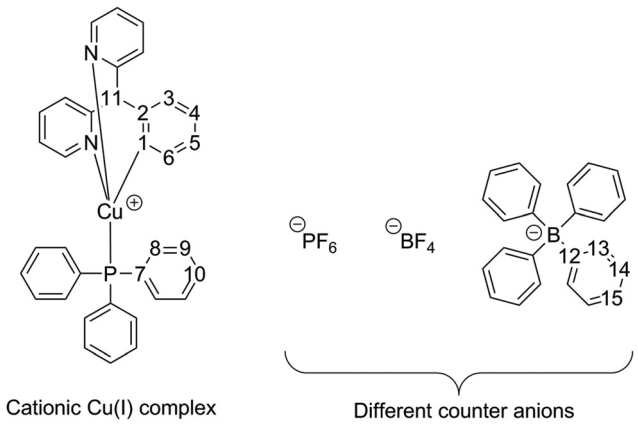

Fig. 7 Numbering of the compounds.

plier (RCA C7164R). For the decay time measurements, the same photomultiplier was used in combination with a FAST ComTec multichannel scaler PCI card with a time resolution of 250 ps. As the excitation source for the decay time measurements, a pulsed diode laser (Picobrite PB-375L) with an excitation wavelength of λ_{exc} = 378 nm and a pulse width <100 ps was used. For absolute measurements of photoluminescence quantum yields at ambient temperature, a Hamamatsu Photonics (C9920-02) system was applied. Doping of polymethylmethacrylate (PMMA) films was performed by dissolving the respective complex (<1 wt%) and the polymer in dichloromethane. After this, the solution was spin-coated onto a quartz-glass plate.

All calculations were carried out with Gaussian09.[104] As the functional B3LYP[85–87] and as the basis set def2-SVP[88,89] were used. As the starting geometry for optimization, a structure obtained from X-ray measurements was used. The optimization of the S_0 and T_1 structures was made by DFT methods and the optimization of the S_1 structure was made by TDDFT methods. No symmetry constraints were applied. Vibrational frequency calculations confirm that all three optimized structures are minima on the potential energy surface.

The data collection for the single crystal structure determinations was performed on a Bruker D8 QUEST diffractometer by the X-ray service department of the Faculty of Chemistry, University of Marburg. The D8-QUEST is equipped with a Mo-K_α X-ray microsource (Incotec), a fixed chi goniometer and a PHOTON 100 CMOS detector. Bruker software (Bruker Instrument Service, APEX2, SAINT) was used for data collection, cell refinement and data reduction.[105] The structures were solved with SIR-97,[106] refined with SHELXL-2014[107] and finally validated using PLATON[108] software, all within the WinGX[109] software bundle. Absorption corrections were applied within the APEX2 software (multi-scan).[105] Graphic representations were created using Diamond 3.[110] C-bound H-atoms were constrained to the parent site. In all graphics the displacement ellipsoids are shown for the 50% probability level, hydrogen atoms are shown with an arbitrary radius. CCDC 1415676–1415678 contain the supplementary crystallographic data for the structures reported in this paper.

Syntheses

General procedure for compounds 1 and 2. The ligand tpym was dissolved in a minimum amount of acetonitrile and $[Cu(MeCN)_4]X$ (X = PF_6 or BF_4) was added. After stirring for 10 min, PPh_3 was added to the solution. The reaction solution was stirred at room temperature for 1 d. The solvent was removed *in vacuo* and the crude product was triturated with diethyl ether (2× with 10 mL). Single crystals were obtained in chloroform by layering with *n*-pentane.

$[Cu(PPh_3)tpym]PF_6$ (1). Prepared from $[Cu(MeCN)_4]PF_6$ (75 mg, 0.20 mmol, 1.0 eq.), tpym (50 mg, 0.20 mmol, 1.0 eq.), and PPh_3 (53 mg, 0.20 mmol, 1.0 eq.) in acetonitrile (8 mL); grey powder. Yield: quantitative. Anal. Calc. for $C_{34}H_{28}CuF_6N_3P_2$ (718.10 g mol^{-1}) C 56.87, H 3.93, N 5.85%; found C 56.46, H 3.84, N 5.68%. ^{1}H NMR (300.1 MHz, $CDCl_3$): δ (ppm) = 8.15 (d, $^3J_{34}$ = 7.8 Hz, 3H, H3), 8.08 (dd, $^3J_{65}$ = 5.1 Hz, $^4J_{64}$ = 1.0 Hz, 3H, H6), 7.82 (ddd, $^3J_{43}$ = 7.8 Hz, $^3J_{45}$ = 7.8 Hz, $^4J_{46}$ = 1.8 Hz, 3H, H4), 7.42–7.64 (m, 15H, H8/H9/H10), 7.15 (ddd, $^3J_{54}$ = 7.8 Hz, $^3J_{56}$ = 5.1 Hz, $^4J_{53}$ = 1.1 Hz, 3H, H5), 6.46 (s, 1H, H11). ^{13}C{^{1}H} (75.5 MHz, $CDCl_3$): δ (ppm) = 155.1 (s, C2), 149.7 (s, C6), 139.6 (s, C4), 133.7 (d, $^2J_{CP}$ = 16.2 Hz, C8), 133.0 (d, $^1J_{CP}$ = 36.4 Hz, C7), 130.9 (d, $^4J_{CP}$ = 1.2 Hz, C10), 129.5 (d, $^3J_{CP}$ = 9.9 Hz, C9), 127.2 (s, C3), 123.6 (s, C5), 57.6 (s, C11). ^{31}P{^{1}H} (101.3 MHz, $CDCl_3$): δ (ppm) = 3.00–8.00 (bs, PPh_3), −143.52 (sept, $^1J_{PF}$ = 713 Hz, PF_6^-). HRMS (ESI+, MeCN): *m*/*z* (%) = 351.0664 (100, $[tpymCu + MeCN]^+$ requires 351.0665), 572.1309 (15, $[tpymCuPPh_3]^+$ requires 572.1311), 310.0404 (6, $[tpymCu]^+$ requires 310.0400). HRMS (ESI−, MeCN): *m*/*z* (%) = 144.9647 (100, $[PF_6]^-$ requires 144.9647). IR (ATR): ν = 1597 (m), 1573 (w), 1473 (w), 1438 (m), 1351 (w), 1305 (w), 1161 (w), 1161 (w), 1096 (w), 1059 (w), 1018 (w), 910 (w), 834 (vs), 783 (m), 750 (m), 696 (m), 648 (w), 619 (m), 556 (m), 529 (m), 501 (m), 423 (m) cm^{-1}.

$[Cu(PPh_3)tpym]BF_4$ (2). Prepared from $[Cu(MeCN)_4]BF_4$ (64 mg, 0.20 mmol, 1.0 eq.), tpym (50 mg, 0.20 mmol, 1.0 eq.), and PPh_3 (53 mg, 0.20 mmol, 1.0 eq.) in acetonitrile (8 mL); beige-colored powder. Yield: quantitative. Anal. Calc. for $C_{34}H_{28}BCuF_4N_3P$ (659.94 g mol^{-1}) C 61.88, H 4.28, N 6.37%; found C 60.60, H 4.41, N 6.40%. ^{1}H NMR (300.1 MHz, CD_3CN): δ (ppm) = 8.18–8.23 (m, 3H, H6), 7.85–7.97 (m, 6H, H3/H4), 7.40–7.70 (m, 15H, H8/H9/H10), 7.25 (ddd, $^3J_{54}$ = 7.5 Hz, $^3J_{56}$ = 5.1 Hz, $^4J_{53}$ = 1.4 Hz, 3H, H5), 6.21 (s, 1H, H11). ^{13}C{^{1}H} (75.5 MHz, CD_3CN): δ (ppm) = 155.5 (s, C2), 151.3 (s, C6), 140.6 (s, C4), 134.5 (d, $^2J_{CP}$ = 16.2 Hz, C8), 134.1 (d, $^1J_{CP}$ = 36.8 Hz, C7), 131.6 (d, $^4J_{CP}$ = 1.2 Hz, C10), 130.3 (d, $^3J_{CP}$ = 9.9 Hz, C9), 126.9 (s, C3), 124.8 (s, C5), 58.6 (s, C11). ^{19}F{^{1}H} (282.4 MHz, CD_3CN): δ (ppm) = −150.97 (s, BF_4^-). HRMS (ESI+, MeCN): *m*/*z* (%) = 351.0656 (100, $[tpymCu + MeCN]^+$ requires 351.0665), 572.1288 (48, $[tpymCuPPh_3]^+$ requires 572.1311), 310.0393 (6, $[tpymCu]^+$ requires 310.0400). HRMS (ESI−, MeCN): *m*/*z* (%) = 87.0034 (100, $[BF_4]^-$ requires 87.0035). IR (ATR): ν = 1597 (m), 1574 (w), 1473 (m), 1438 (m), 1355 (w), 1303 (w), 1287 (w), 1158 (w), 1097 (m), 1053 (s), 1021

 This journal is © The Royal Society of Chemistry 2015

Open Access Article. Published on 09 October 2015. Downloaded on 6/3/2026 2:54:56 PM.
This article is licensed under a Creative Commons Attribution 3.0 Unported Licence.

(m), 1001 (m), 967 (w), 910 (w), 881 (w), 850 (w), 784 (m), 759 (m), 744 (m), 706 (m), 691 (s), 647 (m), 619 (m), 528 (s), 500 (s), 434 (w), 420 (m) cm^{-1}.

[Cu(PPh$_3$)tpym]BPh$_4$ (3). Tpym (50 mg, 0.20 mmol, 1.0 eq.) was dissolved in acetonitrile (5 mL) and CuCl (20 mg, 0.20 mmol, 1.0 eq.) was added. An orange-colored precipitate formed which was converted into a solution by addition of acetonitrile (45 mL). The solution was stirred for 10 min at ambient temperature. Then, $NaBPh_4$ (70 mg, 0.20 mmol, 1.0 eq.) was added. After stirring the reaction solution for 20 min, a fine colorless precipitate formed which was removed *via* a syringe filter. The ligand PPh_3 (53 mg, 0.20 mmol, 1.0 eq.) was added to the filtrate and the reaction solution was stirred for 30 min. Then, the solution was evaporated to dryness and the crude product was triturated with diethyl ether (2× with 10 mL). The product was obtained as a beige-colored powder. Single crystals were obtained in chloroform by layering with *n*-pentane. Yield: 61 mg (0.07 mmol, 35%). Anal. Calc. for $C_{58}H_{48}BCuN_3P$ (892.37 g mol^{-1}) C 78.07, H 5.42, N 4.71%; found C 77.60, H 5.44, N 4.62%. ^{1}H NMR (500.2 MHz, CD_3CN): δ (ppm) = 8.20 (d, $^3J_{65}$ = 4.9 Hz, 3H, H6), 7.81–7.90 (m, 6H, H3/H4), 7.40–7.70 (m, 15H, H8/H9/H10), 7.25–7.33 (m, 8H, H13), 7.21 (ddd, $^3J_{54}$ = 7.1 Hz, $^3J_{56}$ = 5.1 Hz, $^4J_{53}$ = 1.7 Hz, 3H, H5), 6.96 (t, 8H, H14), 6.81 (t, 4H, H15), 6.16 (s, 1H, H11). $^{13}C\{^1H\}$ (75.5 MHz, CD_3CN): δ (ppm) = 164.8 (q, $^1J_{CB}$ = 49 Hz, C12), 155.4 (s, C2), 151.4 (s, C6), 140.6 (s, C4), 136.7 (d, $^2J_{CB}$ = 1.1 Hz, C13), 134.5 (d, $^2J_{CP}$ = 16.7 Hz, C8), 131.6 (s, C10), 130.2 (d, $^3J_{CP}$ = 9.7 Hz, C9), 126.9 (s, C3), 126.5 (q, $^3J_{CB}$ = 2.7 Hz, C14), 124.9 (s, C5), 122.7 (s, C15), 58.8 (s, C11). The quaternary signal C7 of the PPh_3 group could not be observed in the ^{13}C NMR spectrum. HRMS (ESI+, MeCN): *m*/*z* (%) = 351.0657 (100, $[tpymCu + MeCN]^+$ requires 351.0665), 572.1294 (40, $[tpymCuPPh_3]^+$ requires 572.1311), 310.0393 (2, $[tpymCu]^+$ requires 310.0400). HRMS (ESI−, MeCN): *m*/*z* (%) = 319.1663 (100, $[BPh_4]^-$ requires 319.1668). IR (ATR): ν = 1594 (m), 1573 (m), 1499 (m), 1466 (m), 1435 (m), 1364 (m), 1326 (m), 1302 (m), 1264 (m), 1228 (m), 1204 (m), 1179 (m), 1158 (m), 1118 (m), 1094 (m), 1069 (m), 1031 (m), 996 (m), 955 (m), 936 (m), 843 (m), 813 (m), 801 (w), 782 (m), 744 (m), 732 (s), 706 (s), 693 (s), 645 (m), 611 (m), 542 (w), 529 (s), 494 (m), 469 (m), 439 (w), 619 (m), 406 (w) cm^{-1}.

Acknowledgements

The authors thank the German Ministry of Education and Research (BMBF), the European Research Council (ERC), the German Association of Chemical Industry (Verband der chemischen Industrie, VCI), and the German Research Foundation (Deutsche Forschungsgemeinschaft, DFG), GRK 1782 "Functionalization of Semiconductors" for financial support.

Notes and references

1 *Highly Efficient OLEDs with Phosphorescent Materials*, ed. H. Yersin, Wiley-VCH, Weinheim, 2008.
2 *Physics of Organic Semiconductors*, ed. W. Brütting and C. Adachi, Wiley-VCH, Berlin, 2nd edn, 2012.
3 S. Reineke, M. Thomschke, B. Lüssem and K. Leo, *Rev. Mod. Phys.*, 2013, **85**, 1245–1293.
4 C.-L. Ho and W.-Y. Wong, *New J. Chem.*, 2013, **37**, 1665–1683.
5 G. M. Farinola and R. Ragni, *Chem. Soc. Rev.*, 2011, **40**, 3467–3482.
6 P.-T. Chou and Y. Chi, *Chem. – Eur. J.*, 2007, **13**, 380–395.
7 J. Kalinowski, V. Fattori, M. Cocchi and J. A. G. Williams, *Coord. Chem. Rev.*, 2011, **255**, 2401–2425.
8 G. J. A. Williams, S. Develay, D. L. Rochester and L. Murphy, *Coord. Chem. Rev.*, 2008, **252**, 2596–2611.
9 H. Yersin, A. F. Rausch, R. Czerwieniec, T. Hofbeck and T. Fischer, *Coord. Chem. Rev.*, 2011, **255**, 2622–2652.
10 D. Volz, M. Wallesch, C. Flechon, M. Danz, A. Verma, J. M. Navarro, D. M. Zink, S. Bräse and T. Baumann, *Green Chem.*, 2015, **17**, 1988–2011.
11 R. D. Costa, E. Ortí, H. J. Bolink, F. Monti, G. Accorsi and N. Armaroli, *Angew. Chem., Int. Ed.*, 2012, **124**, 8300–8334.
12 R. D. Costa, E. Ortí and H. J. Bolink, *Pure Appl. Chem.*, 2011, **83**, 2115–2128.
13 T. Hu, L. He, L. Duan and Y. Qiu, *J. Mater. Chem.*, 2012, **22**, 4206–4215.
14 M. Wallesch, D. Volz, D. M. Zink, U. Schepers, M. Nieger, T. Baumann and S. Bräse, *Chem. – Eur. J.*, 2014, **20**, 6578–6590.
15 T. A. Niehaus, T. Hofbeck and H. Yersin, *RSC Adv.*, 2015, **5**, 63318–63329.
16 A. Bossi, A. F. Rausch, M. J. Leitl, R. Czerwieniec, M. T. Whited, P. I. Djurovich, H. Yersin and M. E. Thompson, *Inorg. Chem.*, 2013, **52**, 12403–12415.
17 J. W. Facendola, M. Seifrid, J. Siegel, P. I. Djurovich and M. E. Thompson, *Dalton Trans.*, 2015, **44**, 8456–8466.
18 W. Mroz, R. Ragni, F. Galeotti, E. Mesto, C. Botta, L. D. Cola, G. M. Farinola and U. Giovanella, *J. Mater. Chem. C*, 2015, **3**, 7506–7512.
19 M. A. Baldo, S. Lamansky, P. E. Burrows, M. E. Thompson and S. R. Forrest, *Appl. Phys. Lett.*, 1999, **75**, 4–6.
20 M. A. Baldo, D. F. O'Brien, Y. You, A. Shoustikov, S. Sibley, M. E. Thompson and S. R. Forrest, *Nature*, 1998, **395**, 151–154.
21 S. Lamansky, P. Djurovich, D. Murphy, F. Abdel-Razzaq, H.-E. Lee, C. Adachi, P. E. Burrows, S. R. Forrest and M. E. Thompson, *J. Am. Chem. Soc.*, 2001, **123**, 4304–4312.
22 H. Yersin, A. F. Rausch and R. Czerwieniec, in *Physics of Organic Semiconductors*, ed. W. Brütting and C. Adachi, Wiley-VCH, 2012, pp. 371–424.
23 J. Brooks, Y. Babayan, S. Lamansky, P. I. Djurovich, I. Tsyba, R. Bau and M. E. Thompson, *Inorg. Chem.*, 2002, **41**, 3055–3066.
24 Y. Chi and P.-T. Chou, *Chem. Soc. Rev.*, 2010, **39**, 638–655.
25 C.-L. Ho, H. Li and W.-Y. Wong, *J. Organomet. Chem.*, 2014, **751**, 261–285.
26 C. Ulbricht, B. Beyer, C. Friebe, A. Winter and U. S. Schubert, *Adv. Mater.*, 2009, **21**, 4418–4441.

Open Access Article. Published on 09 October 2015. Downloaded on 6/3/2026 2:54:56 PM.
This article is licensed under a Creative Commons Attribution 3.0 Unported Licence.

27 Y. You and S. Y. Park, *Dalton Trans.*, 2009, 1267–1282.
28 G. Tan, S. Chen, N. Sun, Y. Li, D. Fortin, W.-Y. Wong, H.-S. Kwok, D. Ma, H. Wu, L. Wang and P. D. Harvey, *J. Mater. Chem. C*, 2013, **1**, 808–821.
29 T. Fischer, R. Czerwieniec, T. Hofbeck, M. M. Osminina and H. Yersin, *Chem. Phys. Lett.*, 2010, **486**, 53–59.
30 T. Sajoto, P. I. Djurovich, A. B. Tamayo, J. Oxgaard, W. A. Goddard and M. E. Thompson, *J. Am. Chem. Soc.*, 2009, **131**, 9813–9822.
31 R. Czerwieniec, J. Yu and H. Yersin, *Inorg. Chem.*, 2011, **50**, 8293–8301.
32 R. Czerwieniec, K. Kowalski and H. Yersin, *Dalton Trans.*, 2013, **42**, 9826–9830.
33 R. Czerwieniec and H. Yersin, *Inorg. Chem.*, 2015, **54**, 4322–4327.
34 T. Hofbeck, U. Monkowius and H. Yersin, *J. Am. Chem. Soc.*, 2015, **137**, 399–404.
35 M. J. Leitl, F. R. Küchle, H. A. Mayer, L. Wesemann and H. Yersin, *J. Phys. Chem. A*, 2013, **117**, 11823–11836.
36 D. Volz, Y. Chen, M. Wallesch, R. Liu, C. Fléchon, D. M. Zink, J. Friedrichs, H. Flügge, R. Steininger, J. Göttlicher, C. Heske, L. Weinhardt, S. Bräse, F. So and T. Baumann, *Adv. Mater.*, 2015, **27**, 2538–2543.
37 A. Barbieri, G. Accorsi and N. Armaroli, *Chem. Commun.*, 2008, 2185–2193.
38 M. J. Leitl, V. A. Krylova, P. I. Djurovich, M. E. Thompson and H. Yersin, *J. Am. Chem. Soc.*, 2014, **136**, 16032–16038.
39 S. L. Murov, G. L. Hug and I. Carmichael, *Handbook of Photochemistry*, Marcel Dekker, New York, 2nd edn, 1993.
40 C. L. Linfoot, M. J. Leitl, P. Richardson, A. F. Rausch, O. Chepelin, F. J. White, H. Yersin and N. Robertson, *Inorg. Chem.*, 2014, **53**, 10854–10861.
41 J. C. Deaton, S. C. Switalski, D. Y. Kondakov, R. H. Young, T. D. Pawlik, D. J. Giesen, S. B. Harkins, A. J. M. Miller, S. F. Mickenberg and J. C. Peters, *J. Am. Chem. Soc.*, 2010, **132**, 9499–9508.
42 M. Osawa, I. Kawata, R. Ishii, S. Igawa, M. Hashimoto and M. Hoshino, *J. Mater. Chem. C*, 2013, **1**, 4375–4383.
43 M. Osawa, M. Hoshino, M. Hashimoto, I. Kawata, S. Igawa and M. Yashima, *Dalton Trans.*, 2015, **44**, 8369–8378.
44 G. Blasse and D. R. McMillin, *Chem. Phys. Lett.*, 1980, **70**, 1–3.
45 G. Cheng, G. K.-M. So, W.-P. To, Y. Chen, C.-C. Kwok, C. Ma, X. Guan, X. Chang, W.-M. Kwok and C.-M. Che, *Chem. Sci.*, 2015, **6**, 4623–4635.
46 X.-L. Chen, R. Yu, Q.-K. Zhang, L.-J. Zhou, X.-Y. Wu, Q. Zhang and C.-Z. Lu, *Chem. Mater.*, 2013, **25**, 3910–3920.
47 A. Tsuboyama, K. Kuge, M. Furugori, S. Okada, M. Hoshino and K. Ueno, *Inorg. Chem.*, 2007, **46**, 1992–2001.
48 Q. Zhang, T. Komino, S. Huang, S. Matsunami, K. Goushi and C. Adachi, *Adv. Funct. Mater.*, 2012, **22**, 2327–2336.
49 S. Igawa, M. Hashimoto, I. Kawata, M. Yashima, M. Hoshino and M. Osawa, *J. Mater. Chem. C*, 2013, **1**, 542–551.
50 C. Murawski, K. Leo and M. C. Gather, *Adv. Mater.*, 2013, **25**, 6801–6827.
51 Q. Zhang, J. Chen, X. Y. Wu, X. L. Chen, R. Yu and C. Z. Lu, *Dalton Trans.*, 2015, **44**, 6706–6710.
52 H. Ohara, A. Kobayashi and M. Kato, *Dalton Trans.*, 2014, **43**, 17317–17323.
53 C. A. Parker and C. G. Hatchard, *Trans. Faraday Soc.*, 1961, **57**, 1894–1904.
54 T. Gneuß, M. J. Leitl, L. H. Finger, N. Rau, H. Yersin and J. Sundermeyer, *Dalton Trans.*, 2015, **44**, 8506–8520.
55 D. M. Zink, D. Volz, T. Baumann, M. Mydlak, H. Flügge, J. Friedrichs, M. Nieger and S. Bräse, *Chem. Mater.*, 2013, **25**, 4471–4486.
56 D. Volz, M. Wallesch, S. L. Grage, J. Göttlicher, R. Steininger, D. Batchelor, T. Vitova, A. S. Ulrich, C. Heske, L. Weinhardt, T. Baumann and S. Bräse, *Inorg. Chem.*, 2014, **53**, 7837–7847.
57 A. Acosta, J. I. Zink and J. Cheon, *Inorg. Chem.*, 2000, **39**, 427–432.
58 V. Pawlowski, G. Knör, C. Lennartz and A. Vogler, *Eur. J. Inorg. Chem.*, 2005, **2005**, 3167–3171.
59 K. Tsuge, *Chem. Lett.*, 2013, **42**, 204–208.
60 D. M. Zink, M. Bächle, T. Baumann, M. Nieger, M. Kühn, C. Wang, W. Klopper, U. Monkowius, T. Hofbeck, H. Yersin and S. Bräse, *Inorg. Chem.*, 2013, **52**, 2292–2305.
61 H. Araki, K. Tsuge, Y. Sasaki, S. Ishizaka and N. Kitamura, *Inorg. Chem.*, 2005, **44**, 9667–9675.
62 P. Aslanidis, P. J. Cox, S. Divanidis and A. C. Tsipis, *Inorg. Chem.*, 2002, **41**, 6875–6886.
63 V. A. Krylova, P. I. Djurovich, M. T. Whited and M. E. Thompson, *Chem. Commun.*, 2010, **46**, 6696–6698.
64 V. A. Krylova, P. I. Djurovich, J. W. Aronson, R. Haiges, M. T. Whited and M. E. Thompson, *Organometallics*, 2012, **31**, 7983–7993.
65 V. A. Krylova, P. I. Djurovich, B. L. Conley, R. Haiges, M. T. Whited, T. J. Williams and M. E. Thompson, *Chem. Commun.*, 2014, **50**, 7176–7179.
66 P. C. Ford, E. Cariati and J. Bourassa, *Chem. Rev.*, 1999, **99**, 3625–3648.
67 P. M. Graham, R. D. Pike, M. Sabat, R. D. Bailey and W. T. Pennington, *Inorg. Chem.*, 2000, **39**, 5121–5132.
68 O. Horváth, *Coord. Chem. Rev.*, 1994, **135–136**, 303–324.
69 C. Kutal, *Coord. Chem. Rev.*, 1990, **99**, 213–252.
70 N. Armaroli, *Chem. Soc. Rev.*, 2001, **30**, 113–124.
71 N. Armaroli, G. Accorsi, F. Cardinali and A. Listorti, *Top. Curr. Chem.*, 2007, **280**, 69–115.
72 D. V. Scaltrito, D. W. Thompson, J. A. O'Callaghan and G. J. Meyer, *Coord. Chem. Rev.*, 2000, **208**, 243–266.
73 A. Vogler and H. Kunkely, *Top. Curr. Chem.*, 2001, **213**, 143–182.
74 V. W.-W. Yam, K. K.-W. Lo, W. K.-M. Fung and C.-R. Wang, *Coord. Chem. Rev.*, 1998, **171**, 17–41.
75 V. W.-W. Yam and K. K.-W. Lo, *Chem. Soc. Rev.*, 1999, **28**, 323–334.
76 V. W.-W. Yam, V. K.-M. Au and S. Y.-L. Leung, *Chem. Rev.*, 2015, **115**, 7589–7728.

This journal is © The Royal Society of Chemistry 2015

Open Access Article. Published on 09 October 2015. Downloaded on 6/3/2026 2:54:56 PM.
This article is licensed under a Creative Commons Attribution 3.0 Unported Licence.

77 A. Lavie-Cambot, M. Cantuel, Y. Leydet, G. Jonusauskas, D. M. Bassani and N. D. McClenaghan, *Coord. Chem. Rev.*, 2008, **252**, 2572–2584.
78 A. J. M. Miller, J. L. Dempsey and J. C. Peters, *Inorg. Chem.*, 2007, **46**, 7244–7246.
79 O. Moudam, A. Kaeser, B. Delavaux-Nicot, C. Duhayon, M. Holler, G. Accorsi, N. Armaroli, I. Seguy, J. Navarro, P. Destruel and J.-F. Nierengarten, *Chem. Commun.*, 2007, 3077–3079.
80 R. Venkateswaran, M. S. Balakrishna, S. M. Mobin and H. M. Tuononen, *Inorg. Chem.*, 2007, **46**, 6535–6541.
81 A. Robertazzi, A. Magistrato, P. de Hoog, P. Carloni and J. Reedijk, *Inorg. Chem.*, 2007, **46**, 5873–5881.
82 L.-Y. Zou, M.-S. Ma, Z.-L. Zhang, H. Li, Y.-X. Cheng and A.-M. Ren, *Org. Electron.*, 2012, **13**, 2627–2638.
83 G. Accorsi, N. Armaroli, B. Delavaux-Nicot, A. Kaeser, M. Holler, J.-F. Nierengarten and A. Degli Esposti, *J. Mol. Struct. (THEOCHEM)*, 2010, **962**, 7–14.
84 A. Maleckis, J. W. Kampf and M. S. Sanford, *J. Am. Chem. Soc.*, 2013, **135**, 6618–6625.
85 A. D. Becke, *J. Chem. Phys.*, 1993, **98**, 5648–5652.
86 C. Lee, W. Yang and R. G. Parr, *Phys. Rev. B: Condens. Matter*, 1988, **37**, 785–789.
87 B. Miehlich, A. Savin, H. Stoll and H. Preuss, *Chem. Phys. Lett.*, 1989, **157**, 200–206.
88 A. Schäfer, H. Horn and R. Ahlrichs, *J. Chem. Phys.*, 1992, **97**, 2571–2577.
89 F. Weigend and R. Ahlrichs, *Phys. Chem. Chem. Phys.*, 2005, **7**, 3297–3305.
90 D. R. McMillin and K. M. McNett, *Chem. Rev.*, 1998, **98**, 1201–1220.
91 I. I. Vorontsov, T. Graber, A. Y. Kovalevsky, I. V. Novozhilova, M. Gembicky, Y.-S. Chen and P. Coppens, *J. Am. Chem. Soc.*, 2009, **131**, 6566–6573.
92 M. Iwamura, S. Takeuchi and T. Tahara, *Acc. Chem. Res.*, 2015, **48**, 782–791.
93 UV-VIS spectra of neutral bases and their protonated conjugate cationic acids in acetonitrile, http://tera.chem.ut.ee/~manna/spe/base.htm, (accessed July 27, 2015).
94 H. Yersin, H. Otto and G. Gliemann, *Theor. Chim. Acta*, 1974, **33**, 63–78.
95 D. Volz, M. Nieger, J. Friedrichs, T. Baumann and S. Bräse, *Langmuir*, 2013, **29**, 3034–3044.
96 L. Zhang, B. Li and Z. Su, *Langmuir*, 2009, **25**, 2068–2074.
97 Q. Benito, X. F. Le Goff, S. Maron, A. Fargues, A. Garcia, C. Martineau, F. Taulelle, S. Kahlal, T. Gacoin, J. P. Boilot and S. Perruchas, *J. Am. Chem. Soc.*, 2014, **136**, 11311–11320.
98 G. W. Robinson and R. P. Frosch, *J. Chem. Phys.*, 1963, **38**, 1187–1203.
99 W. Siebrand, *J. Chem. Phys.*, 1967, **46**, 440–447.
100 W. L. F. Armarego and D. D. Perrin, *Purification of Laboratory Chemicals*, Elsevier, 4th edn, 1996.
101 R. N. Keller and H. D. Wycoff, in *Inorganic Syntheses*, McGraw-Hill, 1946, vol. 2, pp. 1–4.
102 G. J. Kubas, in *Inorganic Syntheses*, John Wiley & Sons, 1979, vol. 19, pp. 90–92.
103 E. J. Parish, H. Qin, B. H. Lipshutz and T. B. Petersen, in *Encyclopedia of Reagents for Organic Synthesis*, John Wiley & Sons, Ltd, 2001.
104 M. J. Frisch, G. W. Trucks, H. B. Schlegel, G. E. Scuseria, M. A. Robb, J. R. Cheeseman, G. Scalmani, V. Barone, B. Mennucci, G. A. Petersson, H. Nakatsuji, M. Caricato, X. Li, H. P. Hratchian, A. F. Izmaylov, J. Bloino, G. Zheng, J. L. Sonnenberg, M. Hada, M. Ehara, K. Toyota, R. Fukuda, J. Hasegawa, M. Ishida, T. Nakajima, Y. Honda, O. Kitao, H. Nakai, T. Vreven, J. A. Montgomery Jr., J. E. Peralta, F. Ogliaro, M. J. Bearpark, J. Heyd, E. N. Brothers, K. N. Kudin, V. N. Staroverov, R. Kobayashi, J. Normand, K. Raghavachari, A. P. Rendell, J. C. Burant, S. S. Iyengar, J. Tomasi, M. Cossi, N. Rega, N. J. Millam, M. Klene, J. E. Knox, J. B. Cross, V. Bakken, C. Adamo, J. Jaramillo, R. Gomperts, R. E. Stratmann, O. Yazyev, A. J. Austin, R. Cammi, C. Pomelli, J. W. Ochterski, R. L. Martin, K. Morokuma, V. G. Zakrzewski, G. A. Voth, P. Salvador, J. J. Dannenberg, S. Dapprich, A. D. Daniels, Ö. Farkas, J. B. Foresman, J. V. Ortiz, J. Cioslowski and D. J. Fox, 2009.
105 Bruker *AXS*, Madison, Wisconsin, USA, 2012.
106 A. Altomare, M. C. Burla, M. Camalli, G. L. Cascarano, C. Giacovazzo, A. Guagliardi, A. G. G. Moliterni, G. Polidori and R. Spagna, *J. Appl. Crystallogr.*, 1999, **32**, 115–119.
107 G. Sheldrick, *Acta Crystallogr., Sect. A: Fundam. Crystallogr.*, 2008, **64**, 112–122.
108 A. L. Spek, *Acta Crystallogr., Sect. D: Biol. Crystallogr.*, 2009, **65**, 148–155.
109 L. Farrugia, *J. Appl. Crystallogr.*, 1999, **32**, 837–838.
110 K. Brandenburg and H. Putz, *Crystal Impact GbR*, Bonn, Germany, 2012.